TECHNICAL MEMORANDUM

369

Sensitivity of dynamical Seasonal Forecasts to Ocean Initial Conditions

Oscar Alves, Magdalena Alonso Balmaseda, David Anderson, Tim Stockdale

Research Department

11/9/2002

European Centre for Medium-Range Weather Forecasts
Europäisches Zentrum für mittelfristige Wettervorhersage
Centre européen pour les prévisions météorologiques à moyen terme

For additional copies please contact

The Library
ECMWF
Shinfield Park
Reading
RG2 9AX
library@ecmwf.int

Series: ECMWF Technical Memoranda

A full list of ECMWF Publications can be found on our web site under:
http://www.ecmwf.int/publications/

Abstract

The impact of ocean data assimilation on dynamical ENSO forecasting is studied by looking at forecasts started from ocean initial conditions produced with and without data assimilation. Sensitivity is further examined by comparing coupled forecasts started from initial conditions obtained using different ocean forcing fields. A total of four ocean re-analyses for the period 1990-1997, two analyses using sub-surface data assimilation and two using only wind and SST information are considered. Different wind-stress forcing produces significantly different analyses when subsurface data are not assimilated, but these differences are much smaller when sub-surface temperatures are assimilated.

The statistics of the forecast errors show that, with data assimilation, the forecasts of the NINO 3 SST anomaly clearly beat persistence over all lead times (1-6 months), which is not the case when sub-surface ocean observations are not used. The forecasts from the analyses using different wind forcing and no data assimilation differ considerably. The forecasts started from the analyses with data assimilation are generally similar irrespective of which wind product is used, suggesting that data assimilation is effective at reducing the impact of errors in the wind. For both wind forcings, data assimilation improves the forecast skill.

1 Introduction

The importance of ENSO (El Nino Southern Oscillation) for variability of the earth's climate on seasonal to inter-annual timescales has lead to the development of many systems to forecast SST anomalies in the tropical Pacific. These vary widely in complexity, ranging from purely statistical methods to fully coupled dynamical models of the ocean/atmosphere system. Latif et al. (1998) review these methods and their performance for hindcasts of periods in the 1980s and 1990s. Trenberth (1998) reviewed operational and near operational forecasts of the 1997/98 El Nino, concluding that at least for the 1997/98 El Nino, the systems that performed best were based on coupled dynamical models of the ocean and atmosphere. A comparison of forecasts from physically-based models with statistical models for the 1997/8 ENSO is given by Landsea et al 2000, who conclude the opposite; indeed conclude that not one of the physically-based models does an acceptable job.

ECMWF has set up an operational seasonal forecasting system, one of its main aims being the forecasting of ENSO with up to six months lead-time. It is based on a fully coupled ocean-atmosphere model. Some results have already been reported in Stockdale et al.(1998). Forecasting the SST in the tropical Pacific using a fully-coupled model is essentially an initial value problem since predictability resides in information contained in the initial state of the system, particularly the ocean; to some degree land conditions including soil moisture and snow cover and to a lesser degree the initial state of the atmosphere itself may also play a role.

Different techniques have been used to initialise the coupled models. The simplest technique to provide ocean initial conditions is to run an ocean model forced with observed wind stress and with a strong relaxation of the model SST, usually the top level temperature, to observations. This technique would be satisfactory if errors in the forcing fields and ocean model were small. Unfortunately, wind stress products as well as ocean models are known to have significant errors. Recently, assimilation of sub-surface ocean observations into the ocean model has been used to overcome errors in the initial states due to wind forcing or model error. Several institutions have shown that assimilation of sub-surface data leads to initial conditions for the coupled model which produce significantly better results (Ji et al 1996, Wang et al 2001).

This paper discusses the sensitivity of the ENSO forecasts to the ocean initial conditions. In particular the importance of assimilating sub-surface ocean observations, such as from the TOGA-TAO (Tropical Atmosphere Ocean) array, is explored. Also investigated is the sensitivity of the forecasts to initial conditions provided by assimilating the same sub-surface data but using different wind forcing during the assimilation integration. This leads to some possible insights into the sensitivity of the forecasts to errors in the initial state.

This paper is organised as follows. In section 2, the model and the data assimilation scheme used are described. Section 3 compares four ocean analyses over the 1990's produced with and without ocean data assimilation and using two different wind stress forcing fields. Section 4 compares the coupled model forecasts from the four different sets of analyses. In the final section we draw some conclusions.

2 Models and ocean assimilation scheme

2.1 Ocean model

The ocean model used is based on HOPE (Hamburg Ocean Primitive Equation model) version 2 (Latif et al. 1994, Wolff et al. 1997). The model is global and with 20 vertical levels. Horizontal discretisation is on an Arakawa E grid with a variable grid spacing: the zonal resolution is 2.8^o and the meridional resolution varies from 0.5^o in the equatorial region (within 10 degrees of the equator), smoothly increasing to 2.8^o polewards of 30^o. One major difference to the basic version is the calculation of the horizontal pressure gradients at the middle rather than the bottom of each model layer so allowing the sea level gradients to be more consistent with the pressure gradient field. This has been found to be important for sea level assimilation although no such data are assimilated in the experiments reported on in this paper. A second difference is the use of a pseudo ice model to constrain the model solution over the polar regions and a third is the use of a slightly different topography.

The model is forced at the surface with specified fluxes of heat, momentum and fresh water. The solar radiation penetrates below the surface layer exponentially. When the ocean model is run to produce initial conditions for seasonal forecasts, additional relaxation terms for temperature and salt are used to constrain these fields at the surface to prescribed fields as described later. These constraints are not active during the coupled forecasts.

2.2 Ocean data assimilation system

An ocean data assimilation scheme is used to introduce sub-surface observations into the ocean model. It is based on the statistical interpolation scheme described by Smith et al. (1991). This is essentially an optimum interpolation carried out on overlapping sub-domains of the model horizontal grid. Where domains overlap, the analyses are blended together. The breakdown of the globe into sub-domains depends on the observation distribution and is done so that the maximum number of observations within the domain is less than 200. This reduces the cost of matrix inversion, (see Smith et al.1991), though with present computing resources this number could be increased. The optimum equations are solved on each level of the model independently over the top 1000 m. There is no assimilation in the top model level; instead the model SST is relaxed to SST fields derived from the NCEP analysis, with a relaxation time-scale of 3 days. (See Reynolds 1988, Reynolds and Smith 1994, and Smith and Reynolds 1998). A weaker relaxation (time-scale 30 days) was applied to the surface salinity which was relaxed to annual-mean Levitus climatology.

The model background errors are represented by gaussian functions which are anisotropic and inhomogeneous. The values follow Smith et al. (1991). Within 4 degrees of the equator the correlation length scale in the E/W direction is 1500 km while in the N/S direction it is 200 km. In the sub-tropics and high latitudes, polewards of 15 degrees, the correlation length scale is 400 km in all directions. Between the equatorial strip and the sub-tropics there is a smooth transition in correlation scales. Observation errors are assumed to be correlated in space and time, with a spatial correlation function with length scale of 2 degrees and a time correlation scale of 3 days. Since the OI scheme is univariate, the magnitudes of the observation and background errors are not relevant, only the relative ratio which is 1. The observations that were used are from the real-time GTSPP

(Global Temperature Salinity Pilot Project) at NODC (National Oceanographic Data Center). These include data from XBTs (eXpendable Bathy Thermographs), TAO moorings and drifting buoys. A manual quality control procedure was used to remove any observations which were believed to be wrong. Those that passed the quality control were linearly interpolated in the vertical onto model levels for the analysis which was carried out on each level independently.

Observations of temperature were assimilated into the ocean model as it was integrated. Every 10 days the model was stopped and the model state was used as the background for an OI analyses using observations which spanned a window five days either side of the model background. An increment to the background was calculated. To avoid exciting gravity waves, and to allow the model dynamics to adjust gradually to the changes in the density field, this increment was added slowly over the subsequent 10 days, after which a new background field was available, and the cycle repeated. No change was made to the salinity field during the OI assimilation.

2.3 Coupled model

The atmosphere component of the coupled model is the ECMWF NWP IFS (Integrated Forecast System) model version 15R8, with a T63 spectral horizontal resolution and 31 vertical sigma levels. A coupler, OASIS (Ocean Atmosphere Sea Ice Soil coupler) developed by Terray and Thual (1995) was used to interpolate between oceanic and atmospheric grids at coupling times (once per day).

The initial conditions for the atmospheric model were taken from ECWMF re-analyses (ERA-15) for start dates within the period Jan 1991 to Dec 1993 and from the ECMWF operational analyses for start dates thereafter. (ERA-15 only extended to the end of 1993). Land surface conditions such as soil moisture and snow cover were similarly obtained from the atmospheric analysis system. Exactly the same ocean model was used for the coupled forecasts as was used to generate the ocean initial conditions.

3 Ocean analyses for the 1990s

3.1 Details of the analyses

Four analyses from January 1990 to October 1997 were carried out as summarized in table 1. Two experiments in which no sub-surface data were assimilated will be considered as control runs and are denoted C-EC and C-FSU. Two assimilation experiments using the same forcing as in the respective control experiments, but in which sub-surface thermal data were assimilated were also carried out. They are denoted A-EC and A-FSU. The -EC and -FSU experiments differed in the wind stress fields used to force the model. In particular -EC used the surface wind stress fields from the ECMWF Re-analyses (ERA-15) for the period Jan 1990 to Dec 1993 and from ECMWF operational fields from Jan 1994. This combined forcing product will be denoted ERA/Ops. The -FSU experiments used wind stresses calculated from the FSU (Florida State University) winds (O'Brien, J. J., and S. B. Goldenberg, 1982), using a constant drag coefficient, chosen such that the mean of the zonal stress averaged over the equatorial Pacific from 5S to 5N and from 1979 to 1993 matched that from ERA-15; the value of Cd used was 0.00138. As the FSU winds are only available as monthly means within 30 degrees of the equator in the Pacific basin, the high frequency variability (less than one month) from ERA/Ops was added to the FSU stress. ERA/Ops stresses were used outside the area covered by the FSU stresses, with smoothing across the boundary. In all integrations the surface temperature was relaxed to analysed SST as described earlier. The same surface fluxes of heat and fresh water were used in all experiments: these were taken from Era/Ops.

Experiment	Stress Forcing	Assimilation
C-EC	ERA/Ops	none
A-EC	ERA/Ops	Temperature
C-FSU	FSU	None
A-FSU	FSU	Temperature

Table 1: Summary of experiments

3.2 Mean state and seasonal cycle

The equatorial ocean is largely driven by the wind stress forcing from the atmosphere. To first order the pressure gradient due to the thermocline slope is in balance with the wind stress forcing, and so wind stress errors will have a significant impact on the thermocline slope along the equator. Fig 1a shows the annual mean zonal component of the wind stress from the ECMWF analyses for the tropical Pacific. The strongest stresses are associated with the easterly trades at around 15N and 15S, where the stress values are around 0.1 Nm^{-2}. Along the equator the stresses are mainly easterly peaking in the central Pacific, with values around 0.05 Nm^{-2} and decreasing to zero or even reversing direction towards the eastern and western boundaries.

Figure 1b shows the difference between the FSU and the ERA/Ops zonal component of the wind stress. Although the FSU stress product was designed to have the same long-term zonal mean value as the ERA-15 product within 5 degrees of the equator, fig 1b shows that the mean values are in fact not the same. This is because the averaging period for fig 2 is 1991-96. Along the equator the easterly component of the FSU wind stress is stronger than the corresponding ECMWF stress in the central and east Pacific by up to 0.005 Nm^{-2}. The main differences between the two stresses occur in the southern hemisphere in the region of the south-east trades and the region of the South Pacific Convergence Zone (SPCZ) where differences can be in excess of $0.02Nm^{-2}$. In the northern hemisphere the FSU stresses are up to $0.015Nm^{-2}$ weaker than the ECMWF stresses in the west Pacific on the southern edge of the north-east trades but they are stronger than ECMWF in the central and east Pacific. Fig 1c shows the difference between the curl of the FSU wind stress and the curl of the ECMWF wind stress. The differences are large in the southern hemisphere and are not insignificant in the northern hemisphere at around 10N.

The sea level from C-EC is shown in figure 2a, and the difference in sea-level between C-FSU and C-EC is shown in fig 2b. Using FSU stresses as opposed to ERA/Ops leads to a small increase in the equatorial zonal gradient of about 2 cm between the far west and the far east Pacific, compared to a mean gradient of about 40 cm. The stronger sea level gradient in the C-FSU simulation is consistent with the stronger FSU easterlies. Differences increase away from the equator, and are particularly large in the region of the north east trades and SPCZ, where sea level differences of up to 10 cm occur.

Figure 2c shows the sea level difference between the assimilation and control experiments using ERA/Ops stresses (A-EC minus C-EC). In the equatorial band, the sea level stands higher in the experiment in which data have been assimilated: i.e. data have acted to increase the heat content of the upper ocean by deepening the thermocline. The differences in sea level reach up to 6 cm in the central equatorial Pacific. These differences decrease to both east and west and are close to zero in the far east and far west. This means that data assimilation has increased the sea level gradient in the east Pacific and reduced it in the west Pacific. Differences are also large north of the equator, especially between 7N to 10N, where data assimilation has sharpened the thermal gradients. The changes in the northern hemisphere thermal structure imply considerable changes to the north equatorial counter current as discussed in Balmaseda et al 2002. In the southern hemisphere subtropics (10S-20S) the model sea level differs by 8 cm over a wide area.

The large changes seen in fig 2c, especially in the southern hemisphere, might appear surprising given that

this is perceived to be a data poor region. The data coverage for Jan 1996 is given in Fig 3, showing that in fact there is a modest amount of data in the southern hemisphere. To assess the impact of the data, we plot in fig 4 the assimilation increment averaged over the period 1990-1996 along two sections, one at 165E and the other at 140W, together with the difference in mean state between experiments A-EC and C-EC. At 165E the assimilation increment is somewhat asymmetric around the equator, with a tendency to cool the ocean south of 1S. Despite this the subsurface ocean warms uniformly in both the northern and the southern hemisphere. At 140W south of the equator, data assimilation is also non symmetric, but this time it acts to warm the ocean south of the equator. Again, the effect of assimilation is to deepen the thermocline both north and south. In conclusion there is no simple relationship between the increments induced by data assimilation and the differences in thermal structure between assimilation and control. Some of the difference can be accounted for by propagation. These points are discussed in greater detail in Balmaseda et al 2002 and Weaver et al 2002.

In general, differences between control and assimilation are much greater than differences between the two controls indicating that differences in the sea level due to the two wind products are less than the errors in either control. Further, it shows that one of the main impacts of the temperature data assimilation is to correct the model's mean state which might result from errors in the ocean model or the surface forcing, such as the wind stress (Moore and Anderson 1989, Derber and Rosati 1989, Anderson et al 1996).

By comparing fig 2b and fig 2d one can see that the differences in sea level between the two assimilations is significantly less than the difference between the two controls. In the western Pacific between 5 S and 20 S differences between the two controls of up to 10 cm can be seen, whereas the differences between the two assimilations are typically 1cm and seldom more than 3 cm. Although the same thermal data are passed to the two assimilation experiments one should not expect the temperature fields themselves to be identical in the two data assimilation experiments since the weights given to the model first-guess field and to the data are similar, and the former will be affected by the different wind stresses. The two assimilation experiments may also have different salinity structures as there are no constraints on the salinity field during data assimilation. In spite of this, the two assimilations are quite similar.

The mean seasonal cycle, defined as the variation about the annual mean, tells a similar story in terms of the differences caused by different wind products, and the impact of assimilation. For the sake of brevity figures will not be shown, but the most notable features can be summarized as follows.

Both wind products have a similar phase and amplitude of seasonal variability in zonal stress along the equator, but the ERA/Ops winds have a somewhat more spatially-coherent structure. Careful inspection shows that this results in a slightly stronger annual harmonic in the central Pacific. Using the depth of the 20 deg C isotherm (hereafter D20) as a measure of sub-surface variability, both controls show a similarly structured seasonal cycle, with a double peak in January and May, and a minimum in September. The ERA/Ops winds result in a stronger warming (i.e. deeper D20) in May, and stronger cooling in September: the peak to peak signal is about 25m in C-EC, but less than 20m in C-FSU. This is broadly consistent with the differences in wind, although the details cannot easily be related to the wind field differences because of the substantial filtering effect of the ocean.

Differences in the seasonal cycle between the two assimilation experiments are smaller than the differences between the two controls. The difference between the controls and the assimilations is, however, considerably bigger than the difference between the two controls. The assimilation experiments show a weaker seasonal cycle in D20, with the phase shifted slightly to earlier in the year. The May warming is almost eliminated, while the January peak is slightly strengthened. Overall then, we observe that the assimilation of sub-surface data changes the mean seasonal cycle, and reduces the sensitivity of the analyses to uncertainties in the wind.

3.3 Inter-annual variability

In the last section the impact of the assimilation and the differences due to the wind stress on the mean state and the seasonal cycle were described. Perhaps of greater importance is the impact on the interannual variability, since it is the information in the initial state that will provide a forecast different from one year to the next, and it is interannual variability that one is attempting to predict. The inter annual variability in the SST is very similar in all four simulations since it is strongly relaxed to the Reynolds SST (with a relaxation coefficient of 400 $Wm^{-1}K^{-1}$, which corresponds to a relaxation time of about 3 days). The interannual variability in SST from C-EC is shown in figure 5. The dominant features in the SST variability over the period are the warm event of 1991/1992 where the eastern central equatorial Pacific warmed by more than 2.5K, the cold event of 1995/1996 where it cooled by a similar amount and the onset of the major 1997 El Niño. Between these main features there were alternating warm/cold anomalies of a shorter duration and with magnitudes less than 1.5K. Almost all of the variability exceeding 0.5K is to the east of the dateline.

The interannual variability in the zonal wind stress along the equator from ERA/Ops is shown in figure 6a and from FSU in figure 6b. The overall time evolution is similar in both stress fields but the FSU stress has greater variability, particularly in the east. For example, east of 120W the magnitude of the stress anomalies from ERA/Ops is generally less than $0.01Nm^{-2}$, but the magnitude of the stress anomalies from FSU can be double that. There is a strong relation between the large-scale wind stress anomalies in the central Pacific and the SST variability in the east Pacific as can be seen by comparing fig 6 with fig 5. A westerly wind stress is associated with a positive SST anomaly and vice versa.

The differences in the wind stress anomalies from FSU and ECMWF are shown in figure 6c. In the central Pacific differences of up to $0.025Nm^{-2}$ can be seen which are comparable to the size of the interannual anomalies themselves. For example, the 1991/1992 warm event is associated with a westerly wind stress anomaly which can differ by 0.02 Nm^{-2} between the ERA/Ops and the FSU fields. Anomalies in the first six months of 1994 differ by $0.03Nm^{-2}$. Between 1990 and 1993 ERA/Ops generally has weaker easterlies in the central/west Pacific, but from 1994 onwards has stronger easterly anomalies. Differences between these two periods can also be seen in figure 6a where the period 1990 to 1993 is dominated by westerly anomalies while 1995 onwards is dominated by easterly anomalies. Such a long-term change also occurs in the FSU stresses (fig 6b) but not to the same extent. It is very likely that the change from ERA to Operational stresses at the beginning of 1994 contributes to artificial long term variability in the ERA/Ops stresses due to differences in the two analysis systems.

Variability in the stress in the central Pacific leads to perturbations to the thermocline that will propagate eastwards as Kelvin waves. The impact of the different stresses in the central Pacific can be seen in the differences in depth of the 20C isotherm (D20). The differences between the two controls are largest in the east near 110W with differences reaching over 40m and persisting for a few months to a year. These differences can be traced back to the central Pacific two to three months earlier, although amplitudes are significantly lower there, in general less than 10m, where they are associated with wind stress differences. The eastward propagation link can be shown by correlating the differences in D20 between experiments C-FSU and C-EC in the EQ1 region (130W to 90W and 5S to 5N), with the differences in the wind stresses between EC and FSU winds in EQ2 (170W to 130W and 5S to 5N). Fig 7 shows that the correlation peaks at about 1-2 months with EQ2 wind leading EQ1 thermocline depth. This time-scale is commensurate with what one would expect for eastward propagation from the wind-forcing region of EQ2 to the SST response region EQ1, via low mode equatorially-trapped Kelvin waves.

Figures 8a and 8b show the 20C isotherm anomalies from the C-EC and A-EC experiments, respectively. To first order the magnitude of the variability in the east is similar in all four experiments, though the timings of the maxima are not exactly the same. However, in the west Pacific the assimilation shows much stronger

interannual variability, with peaks reaching up to 25m in the assimilation but only up to 5m in the control. Perturbations to the thermocline in the central and west Pacific have a significant impact on the east Pacific, through Kelvin wave dynamics, and through surface projection of these anomalies in the east they can have an impact on the ocean atmosphere system. Therefore sub-surface data assimilation is likely to influence coupled forecasts made with this system. The variability in the two assimilations is very similar and in general the difference is much less than the difference between the two controls, being more or less everywhere less than 10m (not shown). In figs 9a and 9b we show some anomalies at 8N. In the west Pacific there is stronger low frequency variability in the control runs than in the data assimilation experiments, and less high frequency variability.

In general, the low frequency variability in the west Pacific in the control runs has stronger variability off the equator and weaker variability on the equator compared to the assimilations. The weak thermocline variability in the equatorial western Pacific in fig8a suggests that there is not a strong transfer of signal from 8N to the equator.

4 Coupled model experiments

The analyses described above were used to initialise coupled model forecasts out to six months lead time. Forecasts were started on the 1st of January, April, July and October for each year from 1991 to 1997. For each start date and for each analysis described above, an ensemble of five forecasts was created. The ensemble members differed only in that they had small perturbations made to the initial equatorial SST of magnitude 0.01K. Due to the chaotic nature of the atmosphere these perturbations will generate a different sequence of weather events in the different ensemble members. The experiment names used for the analyses, and described in table 1, will also be used to represent the coupled forecasts starting from the respective analyses. This set of forecasts involves 280 years of coupled integration and so represents a significant computational effort, although a larger set with more start months and covering more years would be desirable.

Because of deficiencies in the oceanic and atmospheric models the state of the coupled model drifted with forecast lead time. No attempt was made to reduce this drift during the coupled model integrations with, for example, some form of flux correction. Instead the drift was removed from the coupled model results a postiori, following Stockdale (1997). For a given forecast date, the drift in the system was calculated as the mean error of all the forecasts starting at the same month during the years 1991-1996, but excluding the actual forecast date. Coupled model forecasts for 1997 were not used to calculate the mean coupled model drift as the large anomalies associated with the 1997/98 El Nino may have made the coupled model behave differently to normal. Forecasts for 1997/8 are included in the general statistics shown in figs 11-14 however.

The model SST drift in NINO3 for each of the experiments is shown in fig 10a as a function of lead-time and starting season using the years 1991-6. The smallest drift occurs for forecasts starting in April, where the drift reached around -0.2K after six months for the forecasts initialised with ocean data assimilation. The strongest drift occurs for forecasts starting in October where forecasts initiated without ocean assimilation have a drift which reaches around -3K after six months. In general the forecasts initialised with assimilation have a smaller drift than those without. The forecasts without data assimilation using ERA/Ops forcing in general have a larger drift than those using FSU forcing, with the exception of forecasts starting in July which are very similar. However, differences in the drift between the experiments are considerably less than the mean drift. Figure 10b shows the evolution of the individual forecasts initialized during the period October-1996 to October-1997. The onset of the 97 El Nino was predicted by the forecasts starting on 1 Oct'96, although most experiments produced it too early. The forecasts from the assimilation initial conditions performed better than the control initial conditions for forecasts starting on 1 Oct 1997. The forecasts that started on 1 Jan 97 and 1 Apr 97 did

not capture the rapid warming that occurred during April/May. This was the case both with and without data assimilation. The reason for this deficiency in the performance over this period is probably not related to errors in the initial state, since the forecasts show small sensitivity to the ocean initial conditions. Forecasts from 1 Jul 97 under-predicted the El Nino peak by 0.5-1.0K for all sets of initial states. This underprediction has been considered in greater detail by Vitart et al 2002, who show that it is more related to model error than to an error in ocean initial conditions.

The root mean square (rms) errors for ensemble-mean forecasts with start dates in the period 1991-1997 is shown in fig. 11a for the NINO 3 region, and the corresponding anomaly correlations in fig 11b. In terms of rms error the two sets of forecasts with data assimilation perform significantly better than those without data assimilation. In fact those with data assimilation beat persistence at all lead times. In terms of the rms error statistics, the C-FSU forecasts are better than the C-EC forecasts. The two assimilation experiments are considerable better than the controls for months 1 to 4. The size of the average spread, as measured by the standard deviation of the ensemble is plotted in figure 11a (dotted lines) for all four experiments, showing that the spread is similar whether there is data assimilation or not. Examination of the 4-6 month mean forecast anomalies for the coupled forecasts A-EC and C-EC for individual ensemble members shows that the spread in the five members due to atmospheric noise exceeds 1K for many of the start dates as can be seen in fig 10b for 1997.

In terms of anomaly correlation, the forecasts with data assimilation are better than persistence over all lead times. The forecasts without data assimilation beat persistence at lead times greater than 2 months. At lead times up to 4 months, the forecasts from the two data assimilation experiments A-EC and A-FSU are better than those without data assimilation. The A-FSU not only has the lowest rms error, it also has the highest correlation at all lead times.

Some of the above results can be more clearly seen on scatterplots. Fig 12a compares the data assimilation forecasts from A-EC with those from the control C-EC for both Nino3 and Nino4 regions. This clearly shows the considerable improvement in forecast skill as a result of assimilation. The large diagonal cross marks the centroid of the cloud of small crosses while the length of its arms gives a measure of the reliability. If the centroid is displaced away from the 45 degree line by an amount greater than the cross line, then this indicates that using a Student-t test and assuming the forecast errors are independent for different dates, the displacement is significant at the 95% level. In both the Nino3 and 4 regions this is true. Data assimilation has led to a marked improvement in the skill.

In fig 13 a, b, a comparison is made between the two control forecasts for the NINO3 and NINO4 regions. In both cases the C-FSU is superior to the C-EC. In both figs 12 and 13, there are more large errors in the C-EC than in either A-EC or C-FSU. In fig 14 a,b a comparison is made between the two assimilation forecasts. The relatively close alignment of points along the diagonal shows that individual forecasts are quite similar. This implies that the ocean initial conditions of experiments A-EC and A-FSU are more similar than the other pairs of experiments indicating that assimilation of subsurface temperature is efficient in reducing the uncertainty in the wind.

In summary, without data assimilation the performance of the forecasts is sensitive to the wind stress forcing. Forecasts initialised from the control using FSU wind forcing are better than those initialised from the control using ERA/Ops forcing. Data assimilation constrains the statistics of the forecasts significantly, making them more or less independent of the wind forcing used in the assimilation, at least in terms of the mean statistics for 1991-97. Furthermore, forecasts initiated from data assimilation are in general better than those without data assimilation over the period 1991-97. All forecasts underestimated the strong warming around April/May 1997, suggesting that the problem may not be related to errors in the ocean initial conditions, at least not to errors in the temperature field. Further analysis suggests this is a model error problem.

5 Discussion and conclusions

Four ocean re-analyses for the period 1990-97 have been carried out and a series of forecasts made from these analyses. Two ananlyses used subsurface ocean thermal data and two did not. In all cases the SST was relaxed to observed SST. Two wind products were used to force the ocean model during the analysis stage; one was derived from the ECMWF atmospheric analysis system, the other from FSU. Differences between analyses with and without data assimilation were significantly bigger than differences between analyses using different winds and no data assimilation. One of the main impacts of data assimilation was to correct for errors in the models mean state and seasonal cycle. Despite the drag coefficient being chosen to give the same long-term mean values between FSU and ECMWF stresses in the equatorial Pacific, noticeable differences remained. In the absence of sub-surface data assimilation, FSU forcing produced a better seasonal cycle of the 20C isotherm depth along the equator than did EC forcing. Off the equator the differences in the control runs were large, but these were much reduced when data were assimilated.

There were significant differences in inter-annual anomalies of zonal wind stress between FSU and EC. FSU had variability exceeding 0.02 Nm^{-2} east of 100W while EC had little variability in this region. In the central Pacific, differences in anomalies between the two stresses reached around 0.03 Nm^{-2} with time scales of around 1-4 months. Inter-annual anomalies of the 20C isotherm depth also showed significant differences in the models forced with different stresses. In the east, differences in 20C isotherm depth in the control reached 30 m. The magnitude of the variability in the east Pacific was similar whether data were assimilated or not. In the equatorial west Pacific the assimilation analyses had a significantly stronger variability, reaching 30 m, while the analyses without data assimilation had weak variability, with values generally less than 10 m. Off the equator, the analyses without data assimilation showed stronger variability. The weak anomalies in the equatorial west Pacific without data assimilation are likely to contribute to the lower skill of the forecasts initialised without data assimilation

ENSO forecasting using a fully coupled model depends critically on the initial state of the system for each forecast. This paper examined the importance of ocean initial conditions on the forecasts. Sub-surface data assimilation had a clear positive impact on the NINO 3 SST forecasts over the 1990s. This was especially true when ERA/Ops winds were used to force the ocean model: with data assimilation both rms errors and anomaly correlations of the NINO 3 forecasts were significantly better than persistence over all lead times considered.

Without data assimilation, there was a strong dependence of the forecasts on the wind forcing being used to produce the initial states. With the ERA/Ops wind stresses the NINO 3 forecasts were worse than those using FSU wind forcing in the initialisation and the rms errors were bigger than persistence. Using FSU wind forcing improved the forecast statistics of the control, making the rms errors better than persistence and the anomaly correlations comparable with the forecasts from the assimilation initial conditions. The smaller model drift using FSU wind forcing as opposed to EC wind forcing may be one of the factors contributing to the higher skill of the forecasts initialised using FSU forcing but we have not investigated this.

The onset of the 1997/98 El Nino was reasonably well captured by the forecasts. However, none of the forecasts, neither from assimilation nor ocean-only initial conditions, captured the rapid warming in Nino3 that occurred around April/May 1997. Once the El Nino had developed, forecasts from assimilation initial conditions predicted its subsequent evolution better than those which did not assimilate sub-surface oceanic data.

Acknowledgements

The ocean model was provided by the Max-Planck-Institut fur Meteorologie, Hamburg; ocean data assimilation software by the Bureau of Meteorology Research Centre, Melbourne; and coupling software by CERFACS, Toulouse.

REFERENCES

Anderson D.L.T., J Sheinbaum and K Haines 1996 Data assimilation in ocean models. Rep Prog Phys 59, 1209-1266.

Balmaseda M.et al The ECMWF ocean analysis system. In preparation

Cane M, S.E. Zebiak and S.C. Dolan 1986 Experimental forecasts of El Nino Nature, 321, 827-832.

Derber J.C. and A. Rosati 1989 A global ocean data assimilation system J Phys Oceanogr. 19, 1333-47.

Ji, M., A. Leetmaa, and V. Kousky, 1996. Coupled model predictions of ENSO during the 1980s and 1990s at the National Centers for Environmental Prediction. J. Clim., 9, 3105-3120.

Landsea, C.W., J.A. Knaff, 2000: How much skill was there in forecasting the very strong 1997-1998 El Niño?. *Bull. Amer. Meteor. Soc.*, **81**, 2107-2120

Latif, M., D. Anderson, T. Barnett, M. Cane, R. Kleeman, A. Leetmaa, J. O'Brien, A. Rosati and E. K. Schneider, 1998. TOGA review paper: predictability and prediction. J. Geophys. Res., 103, C7, 14375-14393.

Latif, M., T. Stockdale, J. Wolff, G. Burgers, E. Maier-Reimer, M. Junge, K. Arpe and L. Bengtsson, 1994. Climatology and variability in the ECHO coupled GCM. Tellus, 46A, 351-366.

Moore A.M and D.L.T. Anderson 1989 The assimilation of XBT data in a layer model of the tropical Pacific ocean. Dyn Atmos Oceans 13, 441-464.

O'Brien, J. J., and S. B. Goldenberg, 1982: Atlas of Tropical Pacific Wind stress Climatology 1961-1970, Florida State University, Tallahassee, FL, 187 pp. For more information on updates of the product see: http://www.coaps.fsu.edu/woce/html/pacwinds.htm

Reynolds, R. W., 1988. A real-time global sea surface temperature analyses. J. Climate, 1, 75-86.

Reynolds R.W. and T.M. Smith 1994. Improved global sea surface temperature analyses using optimum interpolation J Climate, 7, 929-948.

Smith T.M. and R.W. Reynolds 1998 A high resolution global sea surface temperature climatology for the 1961-90 base period. J Climate, 11, 3320-3323.

Smith, N. R., J. E. Blomley and G. Meyers, 1991. A univariate statistical interpolation scheme for subsurface thermal analyses in the tropical oceans. Prog. Oceanog., 28, 219-256.

Smith, N. R., 1995: An Improved System for Tropical Ocean Subsurface Temperature Analyses. Journal of Atmospheric and Oceanic Technology: Vol. 12, No. 4, pp. 850-870.

Stockdale, T. N., 1997. Coupled ocean-atmosphere forecasts in the presence of climate drift. Mon. Wea. Rev., 125, 809-818.

Stockdale, T.N., D.L.T. Anderson, J.O.S. Alves, and M.A. Balmaseda, 1998: Global seasonal rainfall forecasts using a coupled-atmosphere model. *Nature*, **392**, 370-373.

Terray L. and O. Thual 1995 OASIS, Cerfacs Technical report TR/GCMC/95-46. See www.cerfacs.fr

Trenberth, K. E., 1998. Development and Forecasts of the 1997/98 El Nino: CLIVAR Scientific Issues. Exchanges; Newsletter of the Climate Variability and Predictability Program (CLIVAR), published by the International CLIVAR Project Office, Max-Planck-Institut fur Meteorologie, Hamburg, Germany.

Vitart F., M. Balmaseda, L. Ferranti and D. Anderson 2002 Westerly wind events and the 1997 El Nino in the ECMWF seasonal forecasting system: a case study. Tech Memo 370.

Wang Guomin, R Kleeman, N Smith, and F Tseitkin 2001, The BMRC coupled general circulation model ENSO forecast system. Monthly Weather Rev in press.

Zhong A, O Alves, A Schiller, G Wang, F Tseitkin and N Smith 2002 A new version of the BMRC coupled ocean-atmosphere general circulation model for seasonal prediction. Available from BMRC, PO Box 1289K, Melbourne, Victoria, Australia.

Weaver A, J Vialard, D Anderson and P Delecluse 2002 Three and four dimensional variational assimilation with a general circulation model of the tropical Pacific. ECMWF Technical Report 365 pp1-74.

Wolff, J., E. Maier-Reimer and S. Legutke, 1997. The Hamburg Ocean Primitive Equation Model. Deutsches Klimarechenzentrum, Hamburg, Technical Report No. 13.

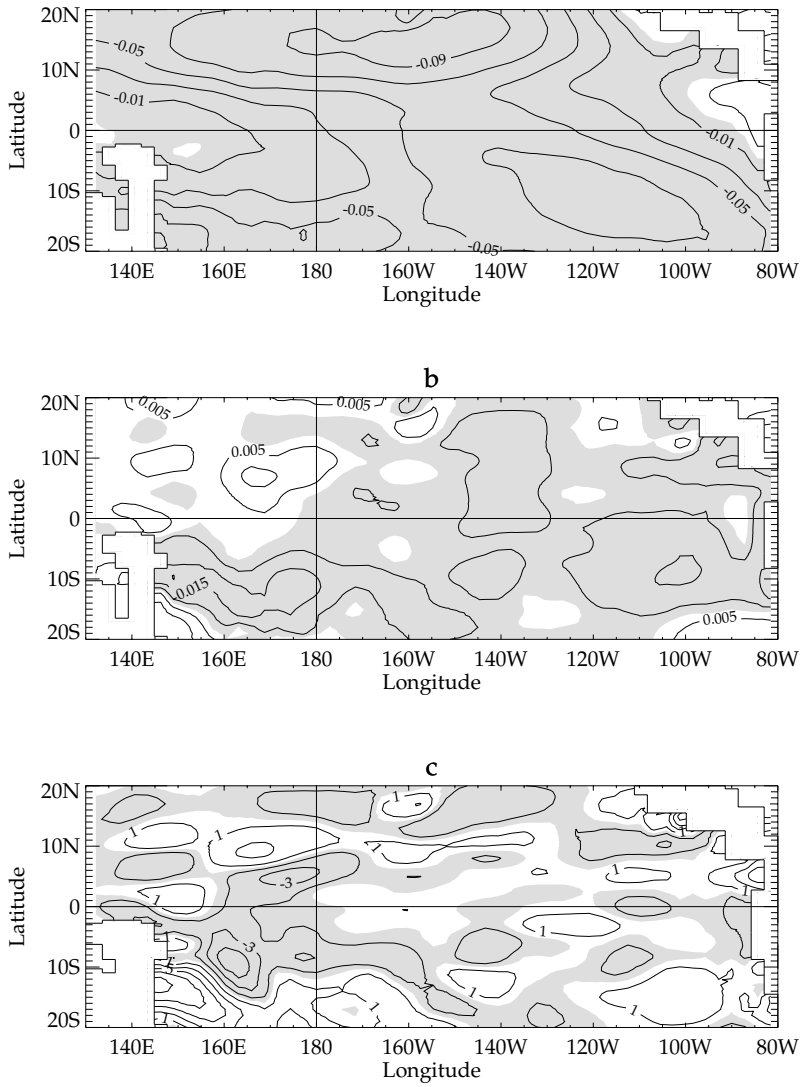

Figure 1: a) Zonal component of wind stress averaged over 1991-96 from the ERA/Ops analyses (c.i. $= 0.02 Nm^{-2}$*) (b) differences in the mean zonal component of the wind stress between the FSU and the ERA/Ops product (c.i.* $= 0.01 Nm^{-2}$*), (c) differences in the mean wind stress curl between FSU and ERA/Ops (scaled by* 10^6*, c.i.* $= 0.02 Nm^{-3}$*). Negative values are shaded.*

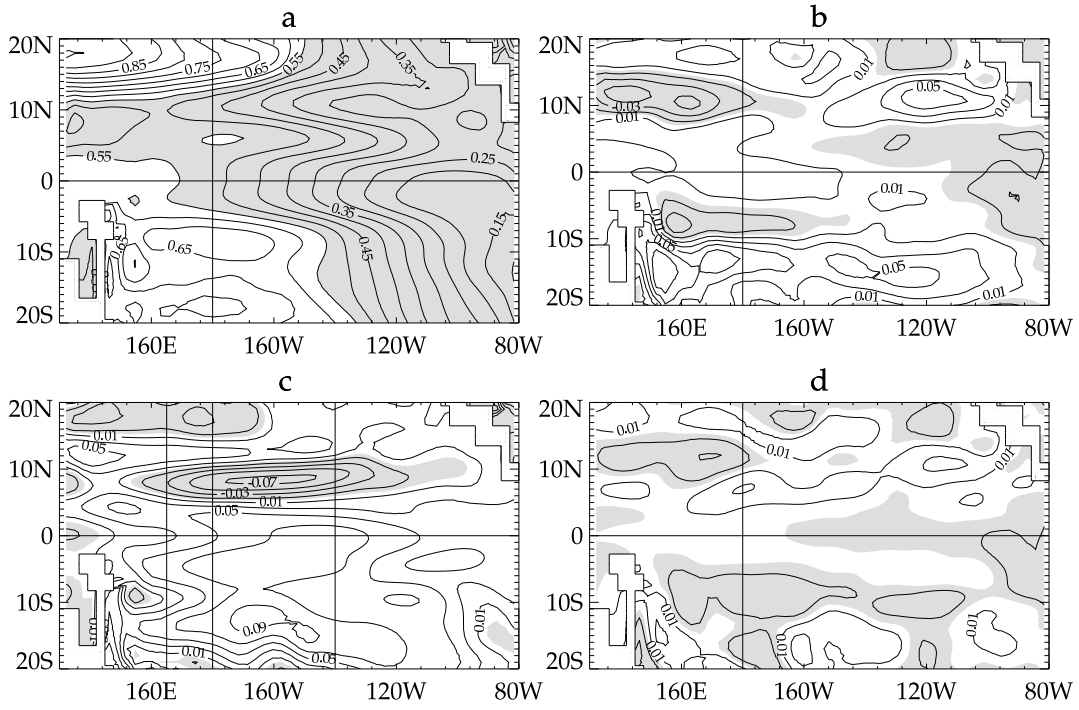

Figure 2: Mean sea level averaged over the period 1991-96 for (a) the control simulation C-EC, (b) the difference in mean sea level between the control simulations C-FSU and C-EC, c) the difference in mean sea level between assimilation and control (A-EC minus C-EC), d) the difference in mean sea level between the two assimilations (A-FSU minus A-EC). The contour interval is 0.05m for a) and 0.02m for b, c and d. In panel a, shading indicates values less than 55cms. In b, c, and d negative values are shaded.

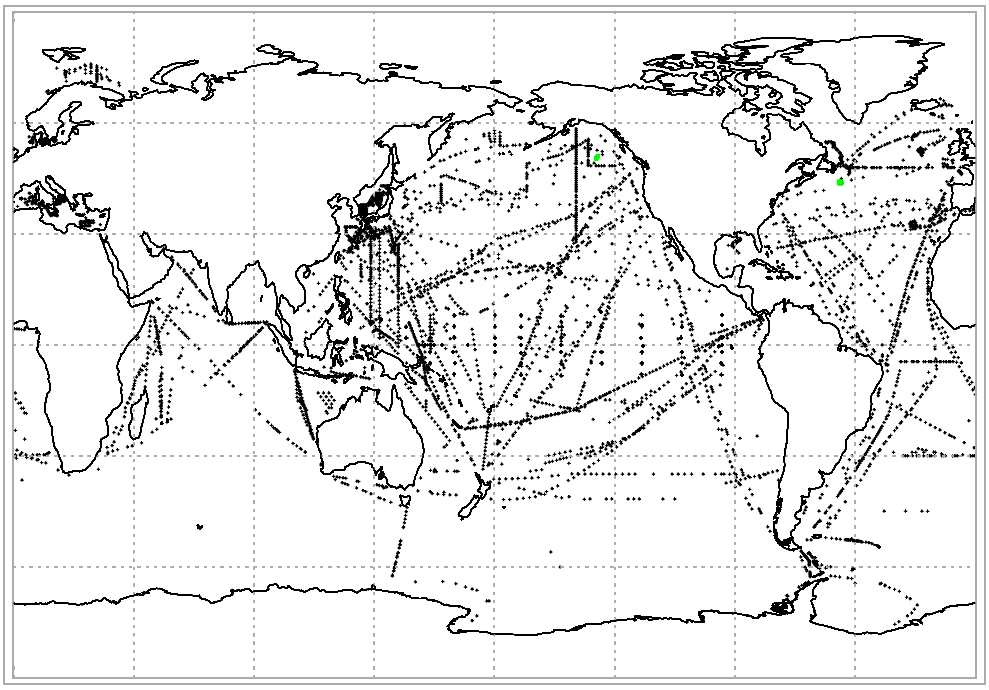

Figure 3: Data coverage for Jan 1996.

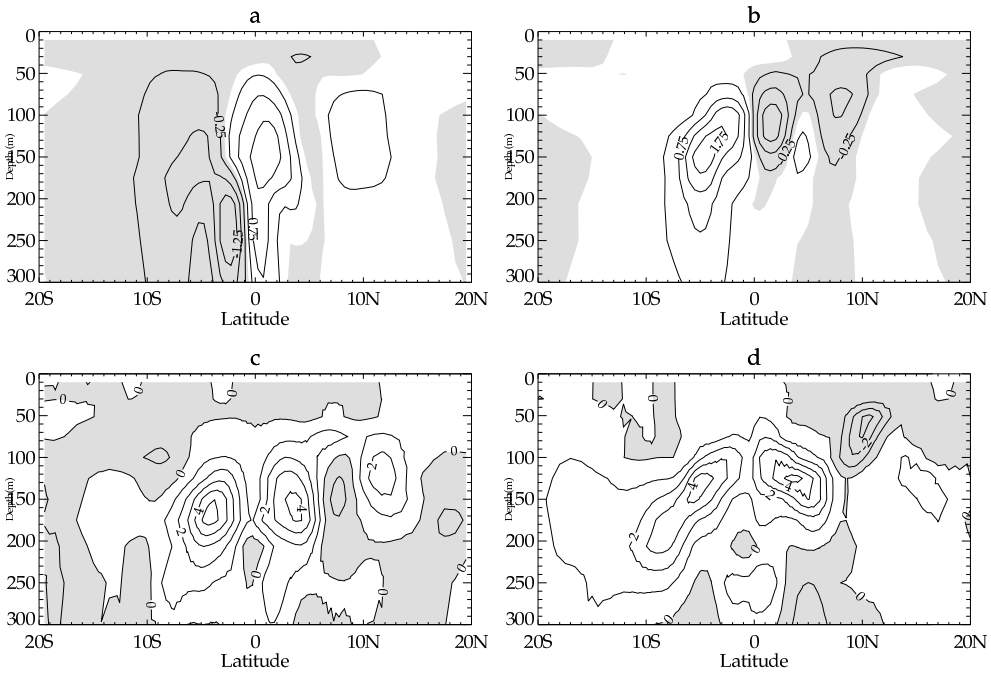

Figure 4: Temperature increment averaged over the years 1990-6 at a) 165E and b) 140W. Contour interval is 0.5 K/month. The lower panels show the 1990-6 average of the differences in temperature between experiments A-EC and C-EC at c) 165E and d) 140W. Contour interval is 1K. Negative values are shaded.

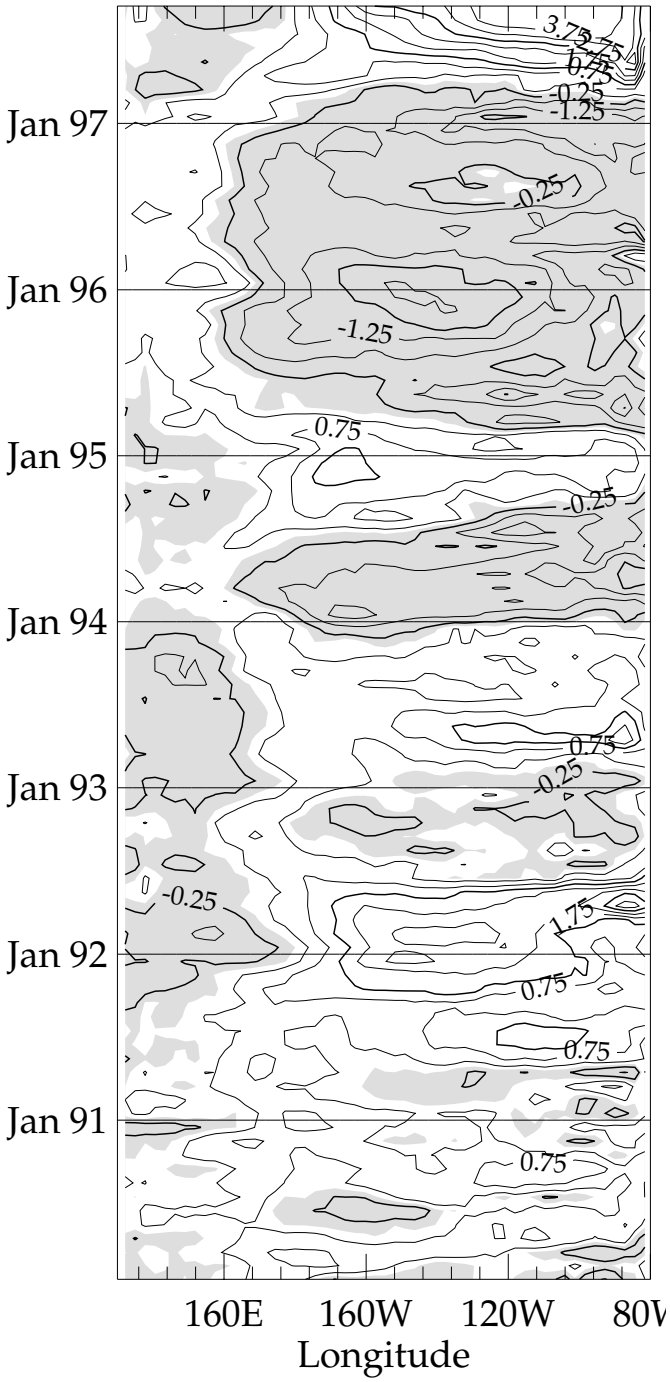

Figure 5: Anomalies of SST along the equatorial Pacific as a function of time over the period Jan 1990 to Dec 1997. Contour interval is 0.5 C. Negative values are shaded

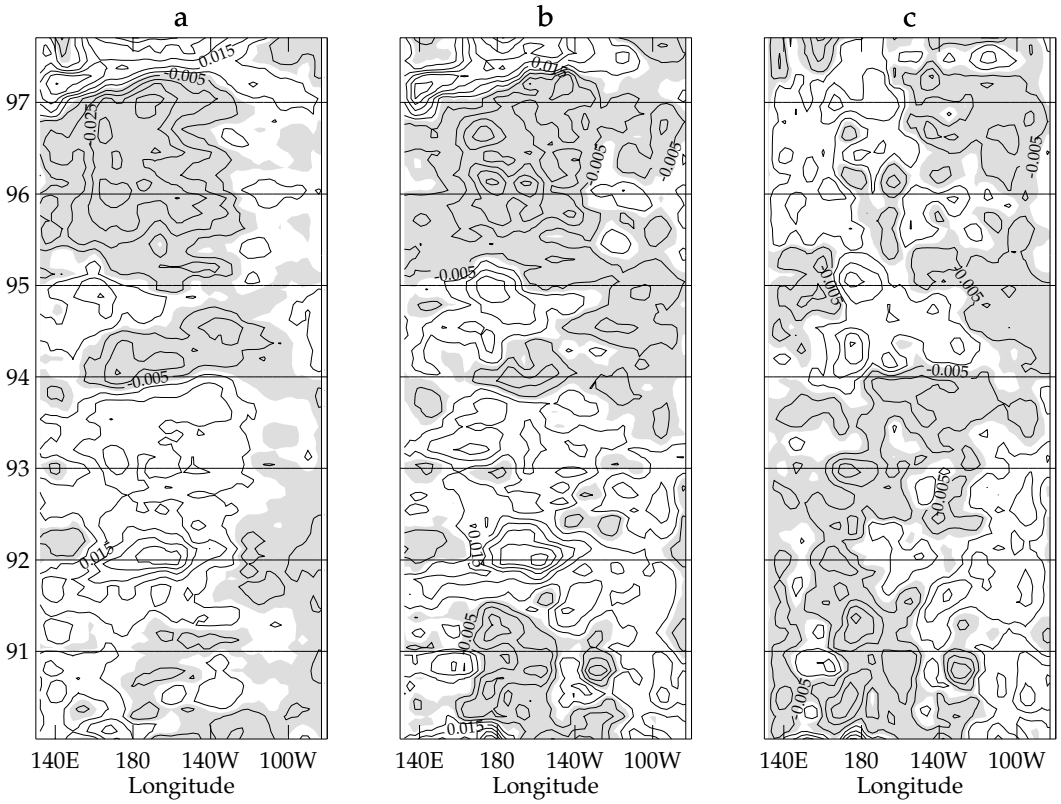

Figure 6: Zonal component of interannual surface stress anomalies: (a) ERA/Ops (b) FSU (c) the difference, FSU minus ERA/Ops. Contour is 0.01 Nm^{-2}. Negative values are shaded

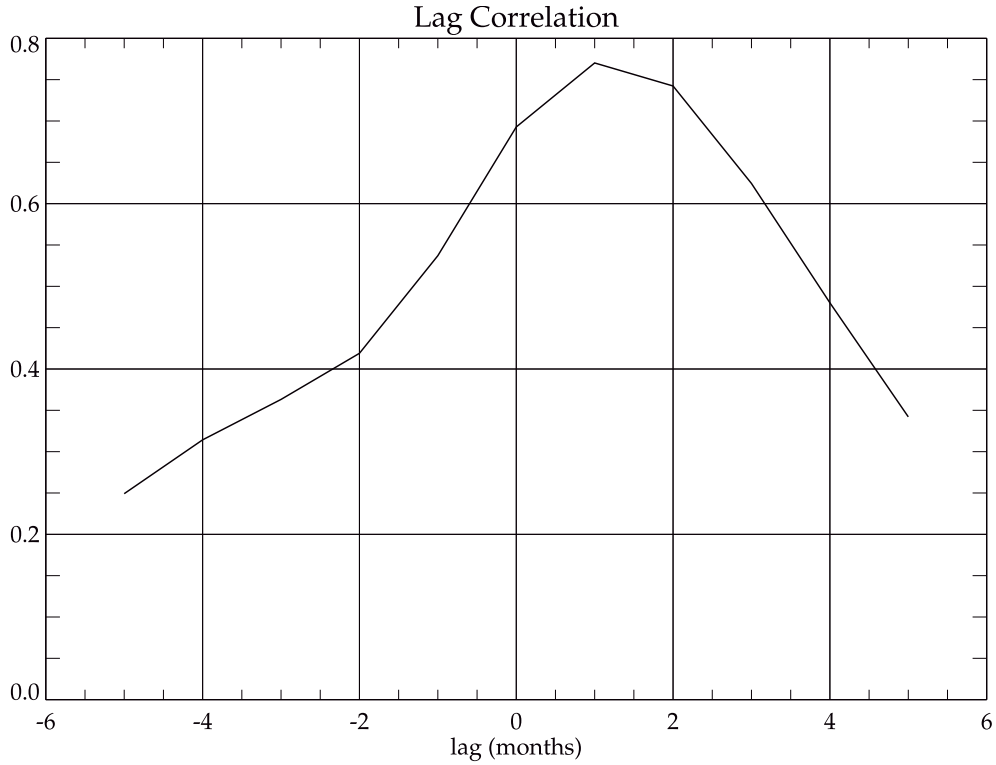

Figure 7: Lag correlation between differences in D20 in EQ1 and differences in the zonal wind stress in EQ2. The differences in D20 are between C-FSU and C-EC. Wind stress differences in the central west Pacific lead sea level differences in the east Pacific.

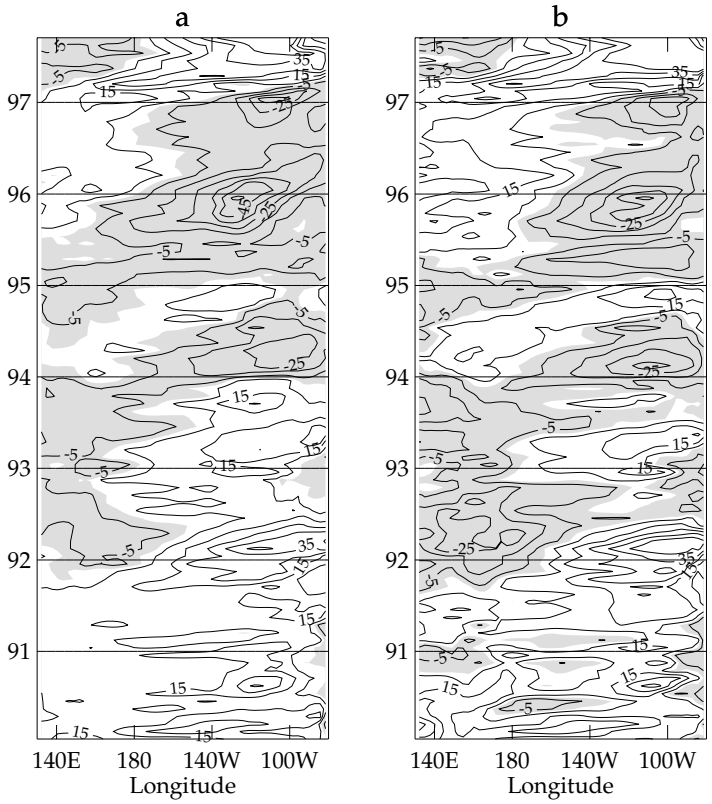

Figure 8: Interannual variability in depth of the 20C isotherm at the equator for: (a) C-EC (b) A-EC. Contour interval is 10m. Negative values are shaded.

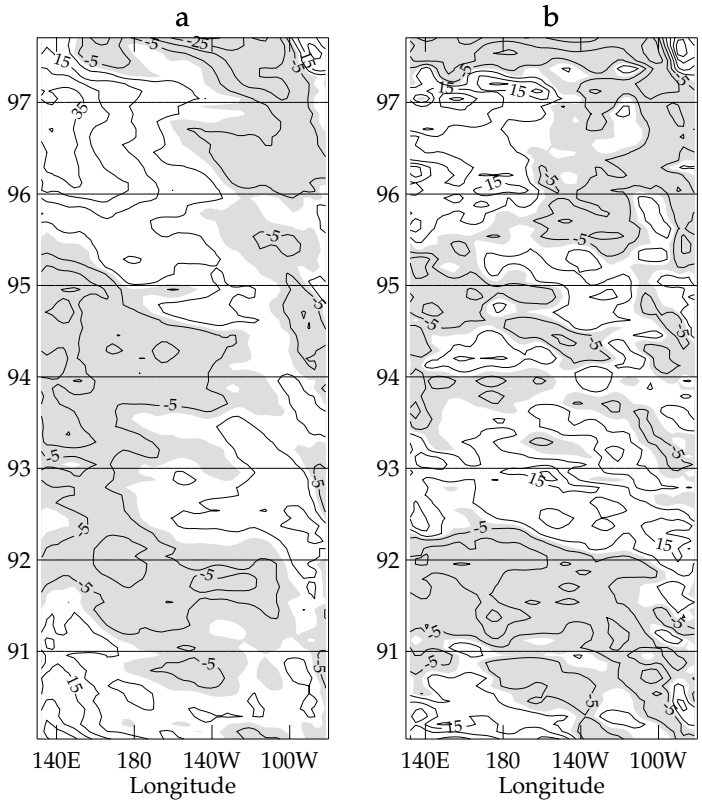

Figure 9: Interannual variability in depth of the 20C isotherm at 8N for a) C-EC and b) A-EC. Contour interval is 10m. Negative values are shaded.

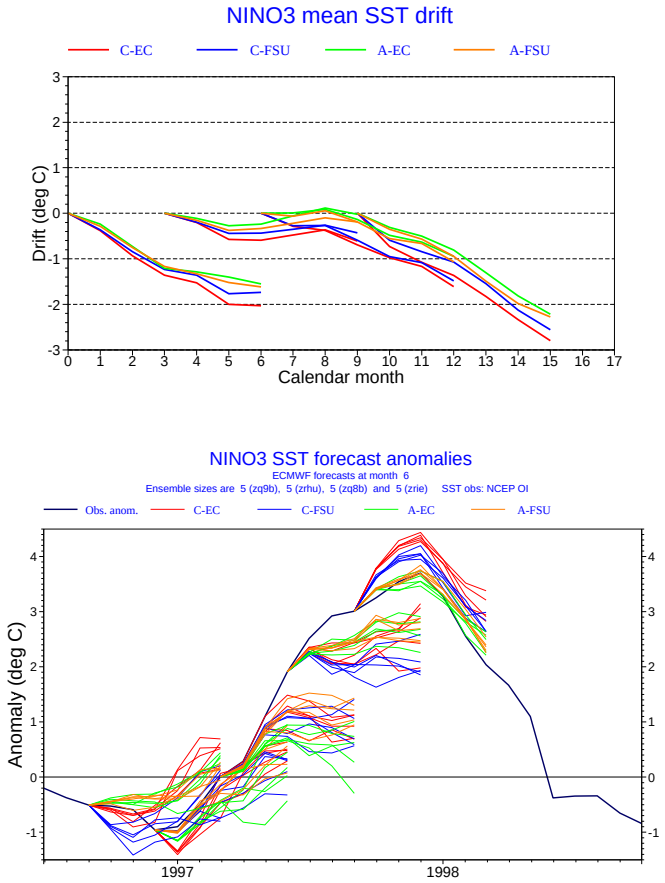

Figure 10: (a) Plot of the mean drift in region NINO3 as a function of start month for the 4 different ocean analyses. The drift is calculated over the period 1991 to 96. (b)Individual forecasts plumes for forecasts initiated in October 1996, January 1997, April 1997, July 1997 and October 1997

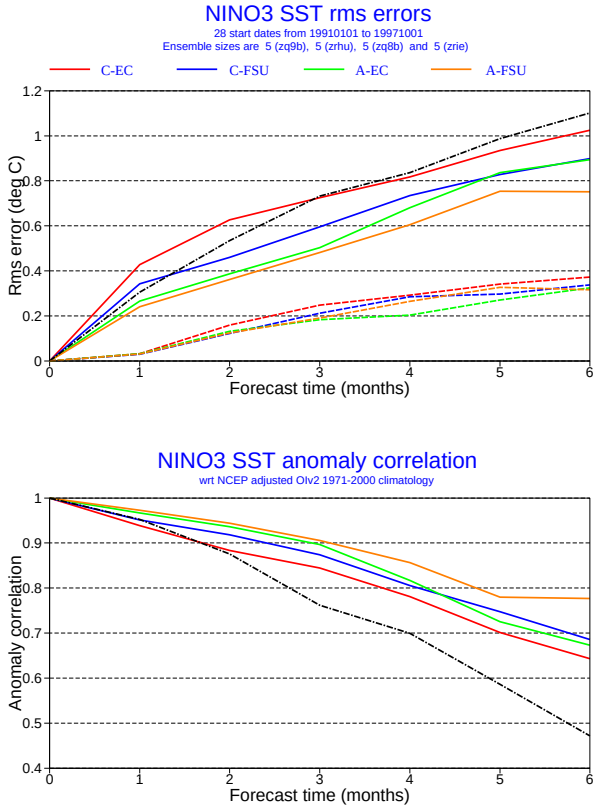

Figure 11: (a) rms error (b) anomaly correlation for the forecasts from 1991-1997 averaged over the 5 member ensemble for the NINO 3 region. Dotted line corresponds to persistence. Dashed lines on upper panel give a measure of the spread of the ensemble. Red C-EC, Blue C-FSU, Green A-EC, Orange A-FSU.

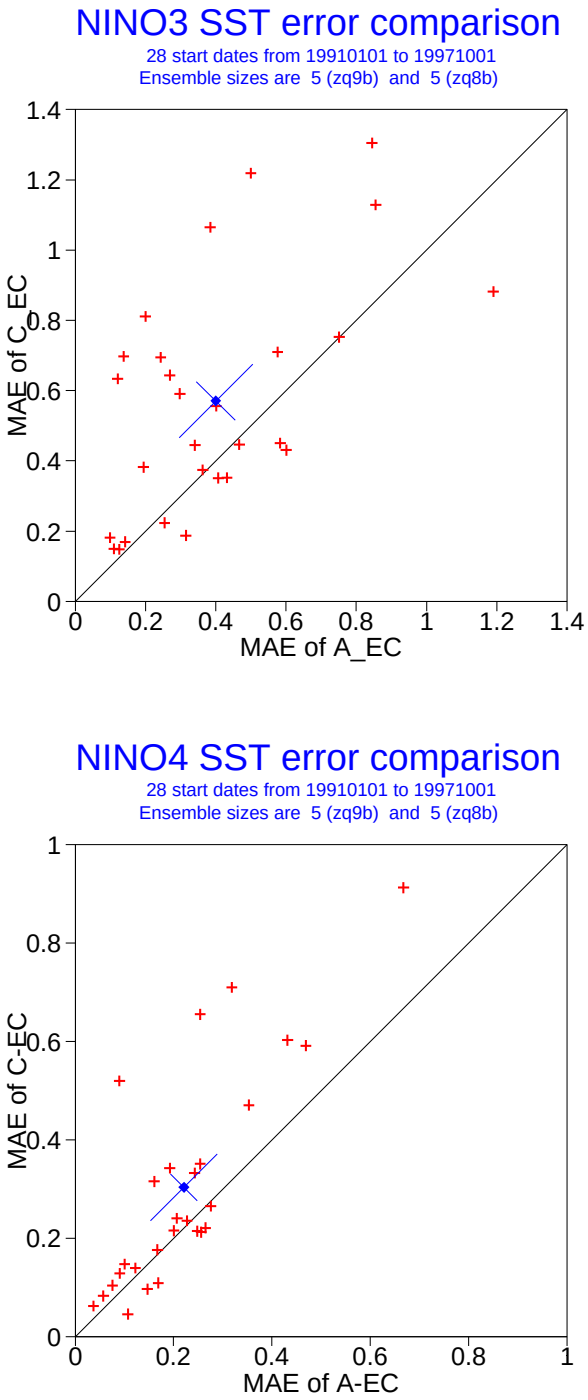

Figure 12: Scatter-diagram of the ensemble-mean absolute SST error averaged over months 1 to 5 for C-EC (vertical) v A-EC (horizontal) covering the period 91-97. The star marks the centroid of the cloud with the arms marking the 95% significance level. In particular, the centroid is displaced away from the diagonal by more than the cross line, meaning that A-EC is superior to C-EC at the 95% significance level. Panel a) is for NINO3 and panel b) is for NINO4.

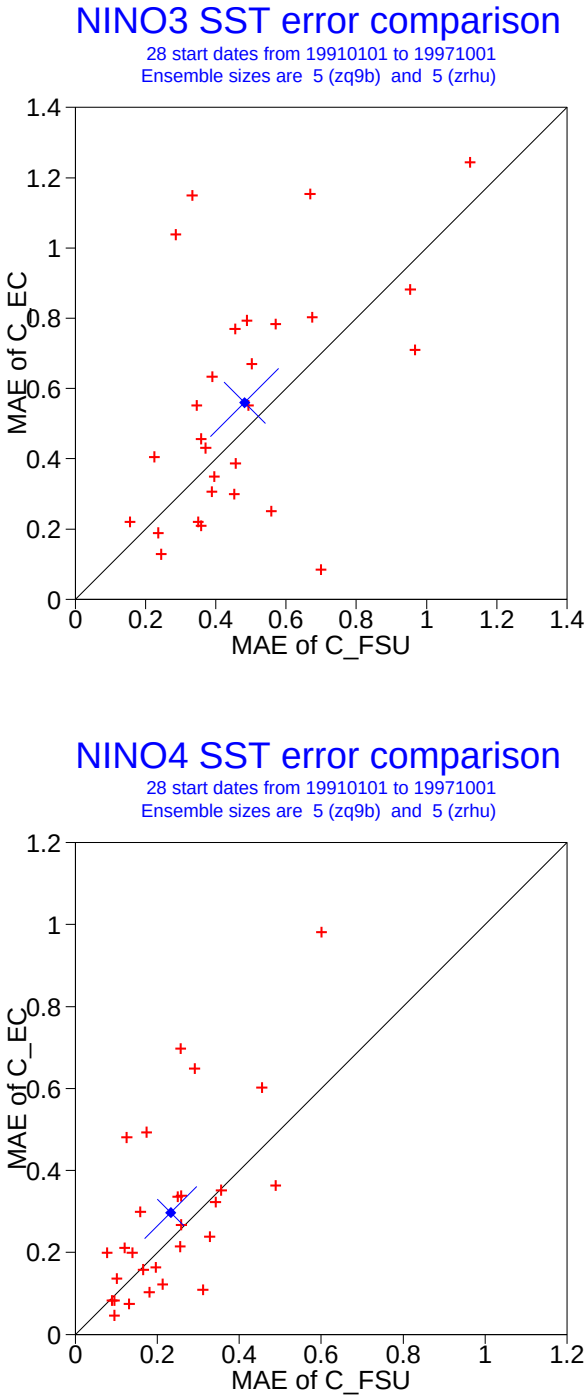

Figure 13: As for fig 12 but a comparison of C-EC against C-FSU. In Nino 4 C-FSU is superior to C-EC at the 95% level. In NINO3 C-FSU also appears to be better than C-EC, though the robustness of this result is less certain.

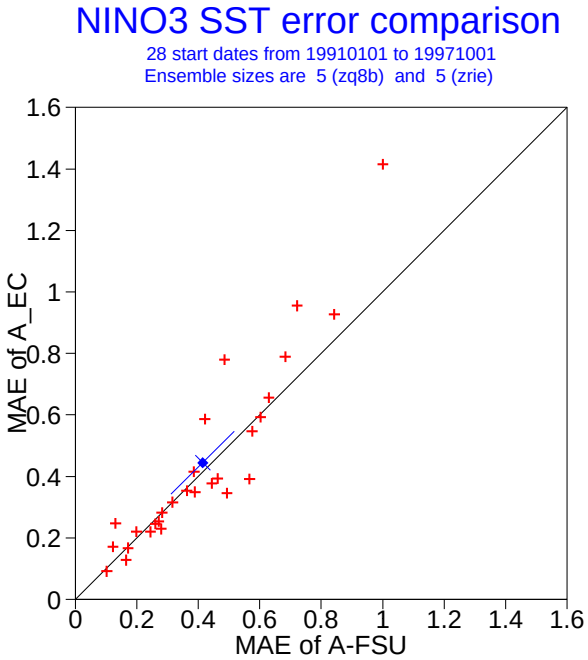

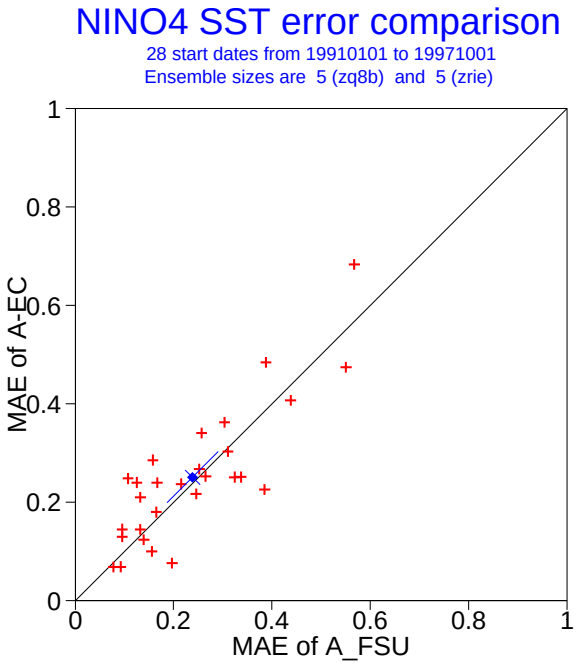

Figure 14: As for fig 12 but a comparison of A-EC against A-FSU. The values align along the diagonal, indicating the data assimilation has reduced the differences shown in fig 13.